Chemical Papers (2024) 78:4875–4890
https://doi.org/10.1007/s11696-024-03437-y

ORIGINAL PAPER

Preparation of biofunctionalized silver nanoparticles using *Clerodendrum glandulosum* leaf extract for evaluation of its antibacterial efficacy

Manmata Dhara[1] · Rubina Khatun[1] · Aditi Mondal[1] · Nazia Kausar[1] · Supriya Mandal[1] · Junaid Jibran Jawed[1] · Mohd Afzal[1] · Abdulla Al Masum[1]

Received: 21 November 2023 / Accepted: 26 March 2024 / Published online: 12 April 2024

Abstract

Antimicrobial resistance (AMR) poses a serious threat to public health on a worldwide scale and has made it extremely difficult to effectively control connected infectious diseases. Due to rapid spread of antibacterial resistance among bacteria, it has become necessary to unveil alternative therapies and medications to combat AMR as commercially available antibiotics are becoming less effective. Recently, nanotechnology has become a fast expanding field with several applications in biomedical sciences. Simultaneously, silver has gained popularity as a comparatively safe antibacterial substance and disinfectant. A wide range of antibacterial, antifungal, and antiviral activities are exhibited by silver nanoparticles. In this current study, *Clerodendrum glandulosum* leaf extract was used for a simple, economical, and environmentally friendly production of biofunctionalized silver nanoparticles for evaluation of antibacterial efficacy. UV–visible spectroscopy confirmed the synthesis of silver nanoparticles giving absorption maxima at 450 nm due to surface plasmon resonance. From the scanning electron microscopy and dynamic light scattering, the average size of the particles was determined to be 150–200 nm. Energy-dispersive X-ray analysis was used to confirm the elemental composition of the biofunctionalized silver nanoparticles. The X-ray diffraction pattern and the Fourier transform infrared spectrogram have confirmed the crystalline nature and successful biofabrication of silver nanoparticles. The MBC values of the silver nanoparticles have been reported to be in the range of 10–20 µg/ml for a fixed population of bacteria, which is significant when compared to the MBC values of gentamicin against the same four strains. Therefore, biofunctionalization of phytoconstituents on nanosurface might improve silver nanoparticles' antibacterial activity as well as their biocompatibility.

✉ Abdulla Al Masum
abdulla.dbs@presiuniv.ac.in

[1] Presidency University Kolkata, Kolkata, India

Graphical abstract

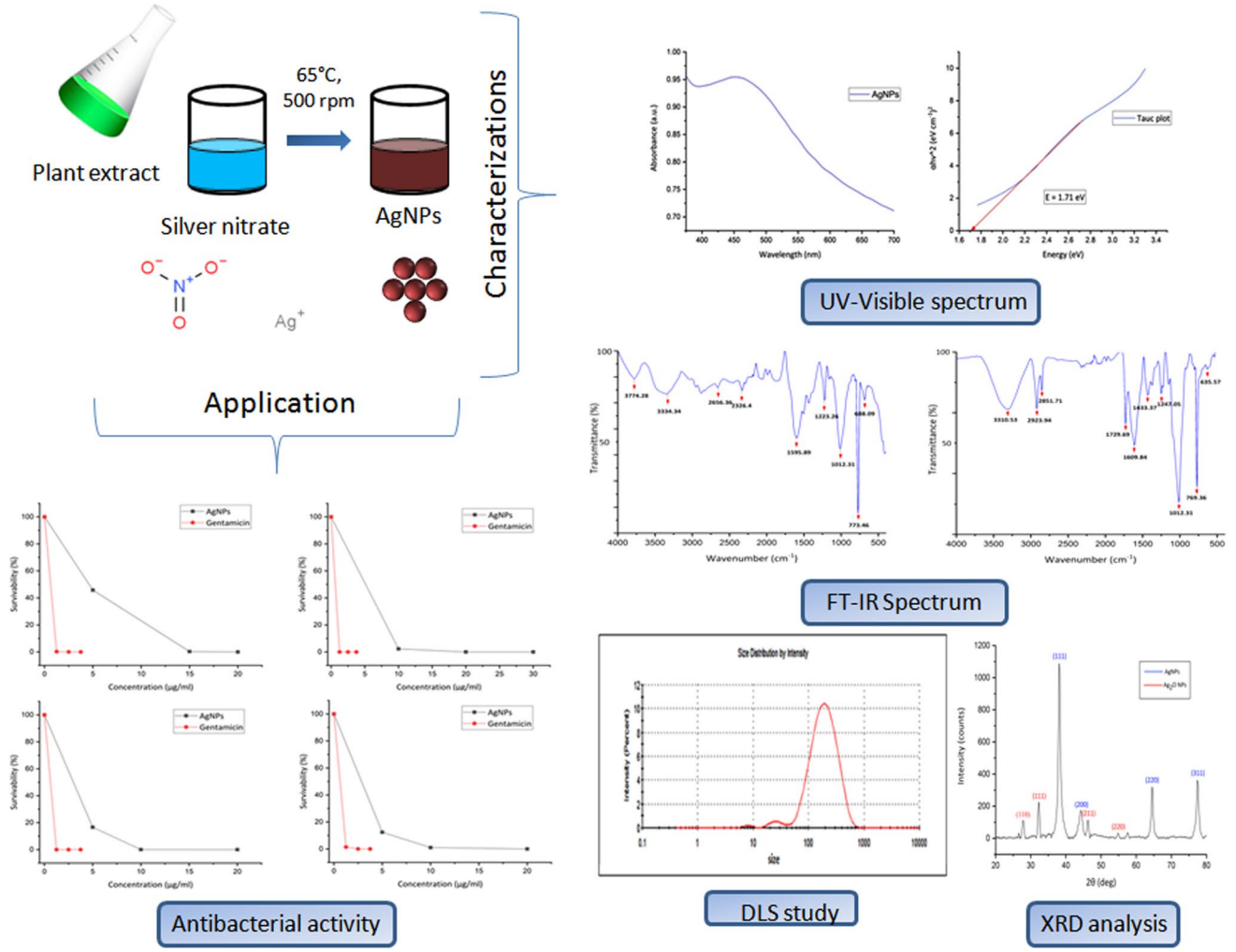

Keywords Antimicrobial resistance · Biocompatibility · Cytotoxicity · Green synthesis · Minimum bactericidal concentration

Introduction

One of the vital threats to the healthcare industry in the current environment is the rise in antibiotic-resistant bacteria. Deadly pathogenic multidrug-resistant bacteria (MDR) are becoming more prevalent every day and represent a major threat to human health (Bharadwaj et al. 2022). Multidrug-resistant bacteria constitute a global concern, increasing morbidity and mortality among infected patients and adversely affecting the prognosis of many different populations, including those receiving cancer therapy, critical care unit treatment, surgery or transplantation (Michael et al. 2014). Antibiotic resistance has been identified as a global issue by the WHO's Global Antimicrobial Surveillance System in a 2017, report estimating a patient with an infection that is resistant to antibiotics is likely to cost around $50,000 to treat, with annual societal expenditures of $20 billion dollars (WHO 2020). This hazard to public health is made worse by the overuse and in some cases misuse of antibiotics as well as the dearth of new medicines entering the pipeline for antibiotics. Due to the emergence of antibiotic resistance, there is a need for increased therapeutic doses have been developed for many commercially available antibiotics. High therapeutic doses and concurrent uses often result in adverse effects and many other undesirable outcomes. Hence, scientists worldwide have been looking for alternates to the traditional chemotherapies or modern strategies to solve this dilemma (Gao et al. 2021).

In the past decade, nanotechnology has been emerging as a multidisciplinary science having wide range of

applications providing solutions to many challenges globally, especially in the field of biomedical sciences. Significant scientific and technological advancements in a variety of sectors, including medicine and physiology, are expected to be produced via nanotechnology and nanoengineering. They can be broadly categorized as the science and engineering involved in the design, synthesis, characterization and application of materials and devices whose smallest functional organization is on the nanometre scale, ranging from a few to several hundred nanometres, in at least one dimension. The spatial and temporal scales under consideration directly influence the possible impact of nanotechnology: Nanoscale engineering refers to the precise control of the arrangement of the constituent molecules and atoms that make up the bulk macroscopic substrate in materials and electronics (Alavi and Rai 2019) This implies that, as a result of the control over their molecular synthesis and assembly, nanoengineered substrates can be made to display very particular and controlled chemical and physical properties in contrast with their lumen matter. These materials and devices can be created to interact with cells and tissues at a molecular (i.e., subcellular) level with a high degree of functional specificity for applications in medicine and physiology, enabling a level of technological and biological system integration that was previously unachievable. In order to bring together the necessary collective expertize needed to develop these novel technologies, traditional sciences such as chemistry, physics, materials science, and biology have come together to form the emerging field of nanotechnology. Due to their extremely small size, nanomaterial have a greater surface to volume ratio that results in the nanoparticles to act as better catalysts (Adil et al. 2022) and also can be biofunctionalized with several molecules such as drugs or ligands that can serve for targeted delivery of drugs.

Different types of nanomaterials are known to exist from ages ago. They include the naturally occurring nanoparticles, such as volcanic ashes and viruses, and human origin, such as diesel exhaust and industrial effluents. There can be incidental nanoparticles (different shapes and sizes) as well as engineered nanoparticles (more well defined; example include metal nanoparticles, quantum dots, nano-capsules, etc.). The research significance of nanoparticles for therapeutic uses has grown over time. The nanoparticles generated are used as biosensors, bioimaging systems and targeted drug delivery systems due to their great stability, biocompatibility, and low toxicity (Hussain et al. 2020). The present period is seeing a surge in interest in metallic nanoparticles, such as gold and silver nanoparticles, due to their better properties and adaptability (Gouyau et al. 2021). Amongst the metal nanoparticles silver nanoparticles (AgNPs) have drawn attention for their application in biomedical sciences as silver exhibits excellent antibacterial activity. There are now three main pathways supported by the literature that have been shown to work either in concert or separately to give AgNPs their antibacterial effects. According to the first theory, AgNPs function at the membrane level because they can pass through the outer membrane and accumulate in the inner membrane, where the nanoparticles' adherence to the cell causes them to become unstable and damaged, increasing the permeability of the membrane and causing cellular content to leak out and ultimately cause the cell to die. Additionally, it has been demonstrated that AgNPs can interact with proteins in bacteria's cell walls that contain sulfur, potentially rupturing the cell wall due to structural damage (Bruna et al. 2021). According to a different theory, Ag^+ ions produced from AgNPs might either engage with sulfur-containing proteins to prevent enzyme activity or with phosphorus moieties in DNA to prevent DNA replication (Fig. 1b) (Sharma et al. 2009). These antimicrobial properties of AgNPs have attracted a lot of interests in the past few years.

Nanoparticles can be synthesized by both chemical as well as biological (green) methods. Chemical approaches require significant investment and have several drawbacks, such as the use of dangerous solvents, the production of harmful by-products, and the uneven surface structure. Chemical techniques are typically made up of multiple chemical species or molecules, which could enhance particle reactivity and toxicity as well as be hazardous to both human health and the environment (Dawadi et al. 2021). For medical and biological applications where the purity of NPs is crucial, biogenic reduction of metal precursors to produce NPs is environmentally benign, less expensive and free of chemical impurities. Similar to chemical reduction, biogenic reduction is a "Bottom Up" technique in which a natural material extract with inherent stabilizing, growth-terminating, and capping properties replaces a reducing agent (Nguyen et al. 2023). Green approaches are non-hazardous, cost-effective, eco-friendly, and easy to approach. Green synthesis of nanoparticles can be done by using plants or by microbes. Plant based approaches are mostly favoured because they are inexpensive, efficient and do not involve the cumbersome process of the isolation of the biomolecules or storing the microbial cultures. In context with the above-mentioned problems, in the present study, leaf extract of *Clerodendrum glandulosum* was being utilized for the synthesis and biofabrication of AgNPs. The herb has historically been used as a vermifuge, anthelmintic, antidiabetic and to treat asthma and malaria fever. *Clerodendrum glandulosum* Leaf aqueous extract is traditionally used by few people of North-East India to alleviate symptoms of diabetes, obesity and hypertension (Singh et al. 1996; Sharma et al. 2001). Terpenes, flavonoids, phenolic glycosides and steroids were extracted from this plant and have been reported to have a variety of biological actions in plant extracts. The phytoconstituents extracted from the leaves act as both reducing

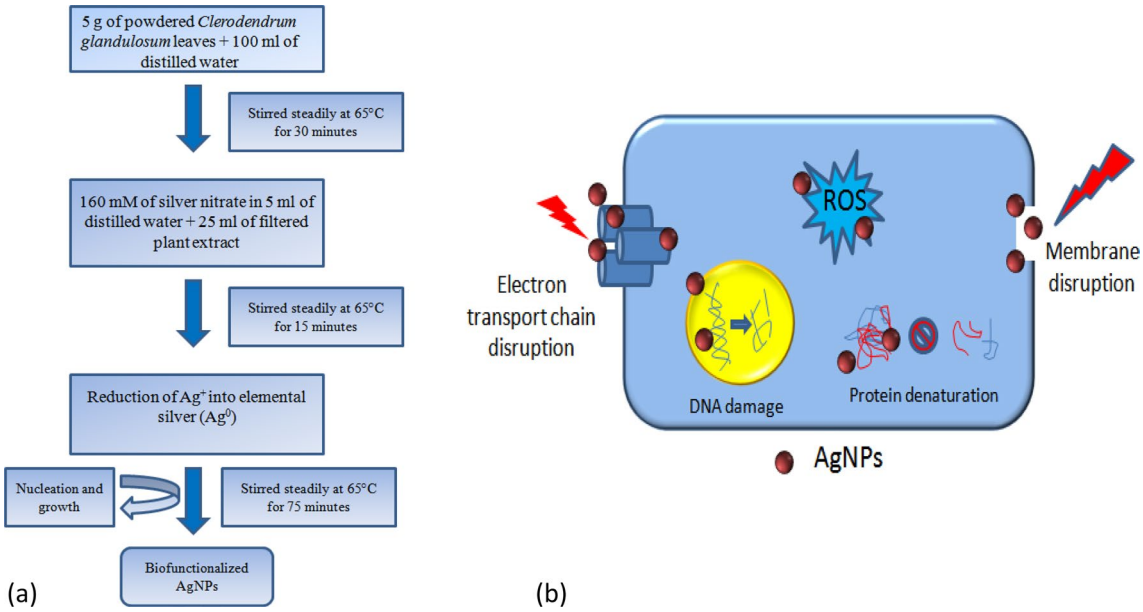

Fig. 1 Flowchart representing synthesis of biofunctionalized AgNPs (**a**) antibacterial mechanism of AgNPs (**b**)

and capping agent enhancing the antibacterial efficacy and biocompatibility of the synthesized AgNPs, as evident in our study.

Result and discussion

UV–Visible spectroscopy

The synthesis of the AgNPs has been carried out at different reaction conditions as mentioned in the Sect. "Experimental". Silver nitrate solution was colourless, whereas the plant extract was pale brown in colour. As the reaction progresses, the solution started to get darken and eventually a dark brown colloidal suspension was formed, indicating the synthesis of the AgNPs as depicted in Fig. 2. This colour change is attributed to the surface plasmon resonance, an optical property signature to the noble metals (Ibrahim 2015). To further confirm the synthesis of biofunctionalized AgNPs, UV–visible spectroscopic analysis has been employed. The reaction initially was carried out at different reaction conditions such as different concentration ratios of the reactants, different temperature and pH.

Eventually, it was optimized that the best possible synthesis was observed when the concentration ratio was 9.25 (plant extract to silver nitrate solution), pH around about 5 and 65 °C temperature (Fig. 3a). However, when the concentration ratio was kept to 5.56, a partial synthesis was observed. To confirm the synthesis of AgNPs, samples were collected at different time interval and subjected to UV–Visible spectroscopic analysis. When the concentration ratio and the pH were kept to 9.25 and 5, respectively, synthesis began since half an hour from the commencement of the reaction. The reaction was seemed to be completed after 60 min as no further change in the UV–visible spectrum was noticed (Fig. 3b).

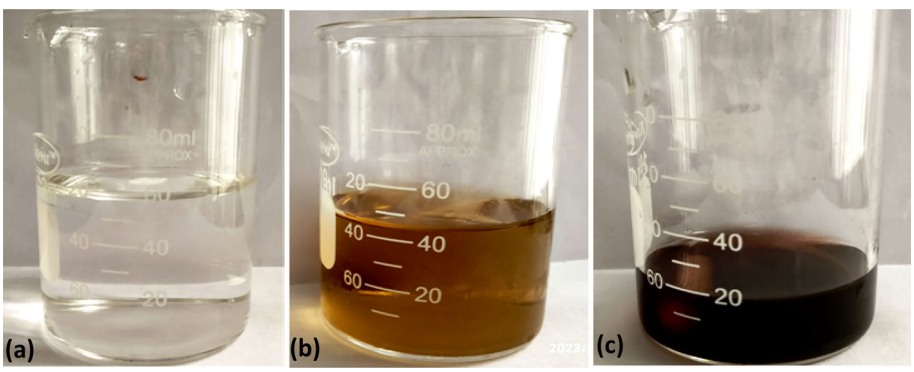

Fig. 2 Visual observation of colour change during AgNPs green synthesis; silver nitrate solution (**a**), plant extract (**b**) and Biofunctionalized AgNPs (**c**)

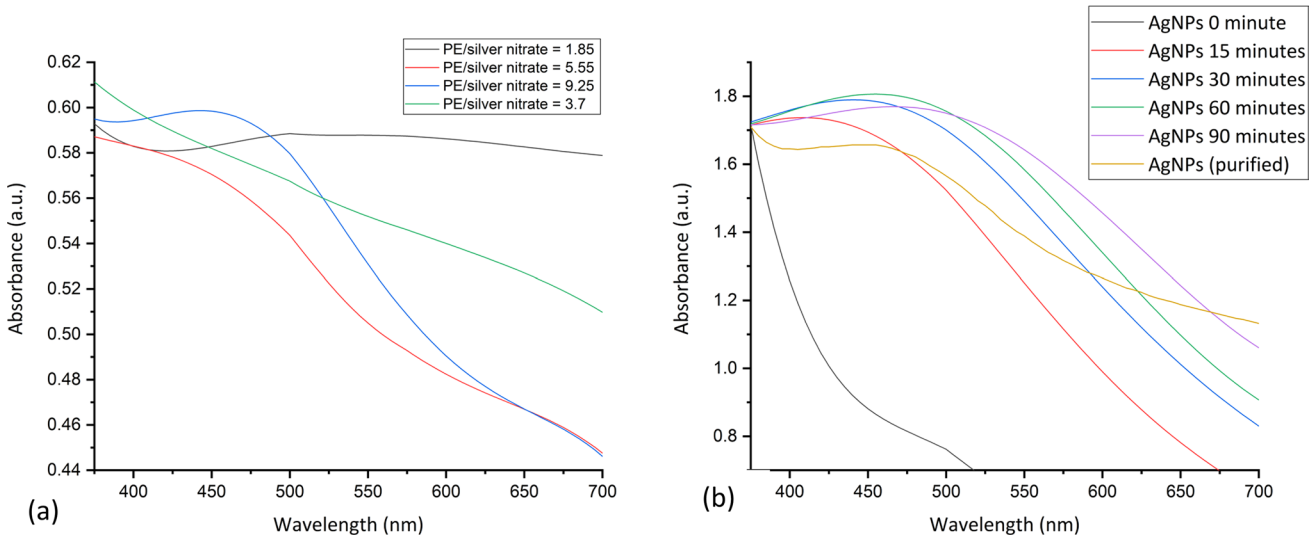

Fig. 3 UV–Visible plot of green synthesis of AgNPs under different concentration ratios of plant extract to silver nitrate (**a**) and different time intervals at pre-optimized concentration ratio (**b**)

Further keeping the reaction to continue has resulted in aggregation and partial oxidation of nanoparticles turning the solution colour from dark brown to black signifying formation of silver oxide crystals as evident in the X-ray diffraction (XRD) analysis. The synthesized biofunctionalized AgNPs shown to have significant stability up to 1 month. When the AgNPs was kept at 4 °C at 1 mg/ml concentration, no significant change in the UV–Visible spectrum was observed. However, prolonged storage or improper storage lead to aggregation of nanoparticles, size variability and alteration in the biophysical properties that was evident from broadening of the SPR peak. After the completion of synthesis and purification of the sample through centrifugation, the purified sample was washed three times with distilled water and the UV–visible data was recorded. The UV–visible absorption spectrum of the synthesized AgNPs as depicted in Fig. 4a showed a broad absorption maxima at around 450 nm due to surface plasmon resonance of the AgNPs (Ahmad et al. 2011). The slight broadness of the peak signifies the aggregation of the nanoparticles, partial oxidation to silver oxide and little size variability. From the UV–visible data, direct band gap energy was calculated by Tauc plot. To calculate the band gap energy, the following equation has been

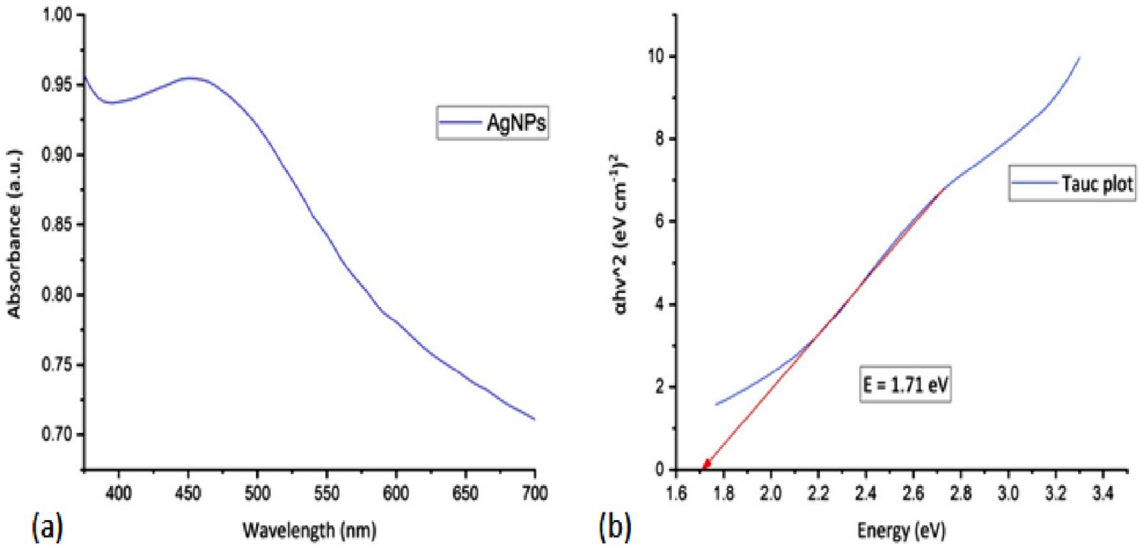

Fig. 4 UV–Visible plot of biofunctionalized AgNPs (**a**) and Tauc plot for direct band gap energy calculation (**b**)

used depicting the relationship between photon energy and absorption coefficient (Feng et al. 2015).

$$\alpha hv = B(hv - E_g)^{0.5} \quad (1)$$

In Eq. (1), 'α' is the absorption coefficient, 'hv' is the photon energy and 'B' is a constant that is independent of photon energy. The E_g-value of AgNPs can be determined by plotting the $(\alpha hv)^2$ against hv followed by taking the intercept of the plot on the x-axis. The band gap energy was calculated to be 1.71 eV.

It has previously been reported by Mistry et al. (2021) that the band gap energy of AgNPs was 2.48 eV. Aziz et al. (2018) reported that silver nanoparticles synthesized using sol–gel method has band gap energy of 2.5 eV. In our study, the determined band gap energy was 1.71 eV.

When the particle size approaches the nanoscale, where each particle is composed of a very small number of atoms or molecules, the band's width narrows and there are fewer overlapping orbitals or energy levels. The energy gap between the conductor and the voltage band will widen as a result. This explains why NP has a larger energy gap than the corresponding bulk matter. As a result, the NP show less electrical conductivity than the bulk material that was used to make them. As a result, during green synthesis, the absorption spectrum shifts towards lower wavelengths. In our study, as the band gap energy is less compared to that of the recently reported values, it can be expected that there is a heterogeneity in the particle size which happens often during the green synthesis due to presence of various surfactants in different proportions. A larger band gap energy means that more energy is required to excite an electron from the valence band to the conduction band and hence light of a higher frequency and lower wavelength would be absorbed. Therefore, a red shift in the surface plasmon resonance of the AgNPs was observed in our study (Fig. 4b). This shift in the band gap can be attributed to nanoparticles' surface chemistry due to fabrication of phytoconstituents.

Fourier Transform Infrared Spectroscopy (FTIR)

The study of vibrational energies upon infrared excitation of the synthesized biofunctionalized AgNPs were carried out by FTIR spectroscopic analysis. Figure 5a depicts the FTIR spectrum of synthesized biofunctionalized AgNPs whereas Fig. 5b shows the same for plant extract. Several peaks have been observed due to bond vibrations of the phytoconstituents.

The strong band at 3374.28 and 3310.53 cm^{-1} are attributed to the O–H stretching of alcohols and phenols. The strong and sharp bands at 2923.24 and 1609.84 cm^{-1} corresponding to the C–H stretching vibration in alkanes and C=C stretching vibration in alkenes, respectively. The bands at 1729.69 and 1247.05 cm^{-1} can be attributed to C=O stretching in aldehydes and esters and C–O stretching in aromatic esters, respectively. The C–H bending vibration is attributed to peaks at 769.36 and 773.46 cm^{-1} from aromatic groups. The bands at 1012.31 cm^{-1}can be attributed to C–O stretching from alcohols (Priya et al. 2011; Marimuthu et al. 2011). The similar banding pattern for C–H (alkanes), C–O (alcohols), C–O (aromatic esters), O–H (phenols), O–H stretching, and methyl group observed in both the spectra

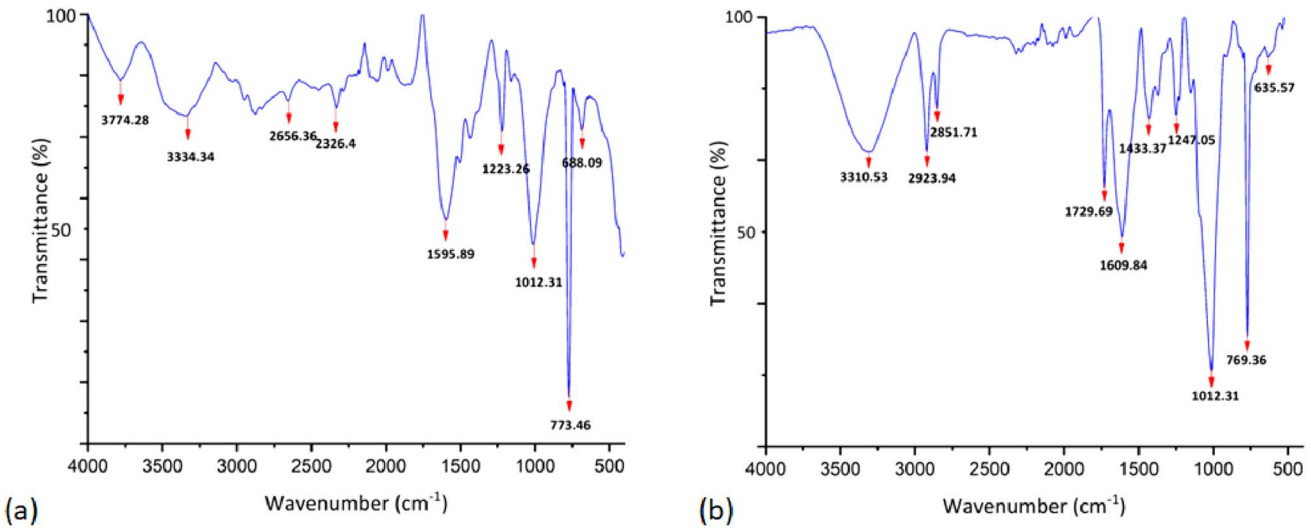

Fig. 5 FTIR analysis of biofunctionalized AgNPs (**a**) and plant extract (**b**)

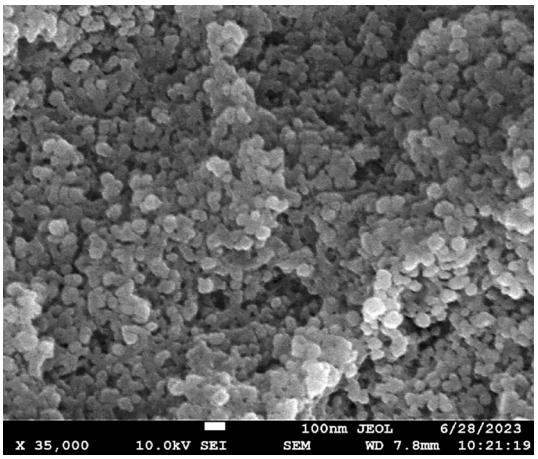

Fig. 6 Scanning electron microscopy of biofunctionalized AgNPs

and the minor shifts in the position confirms the presence of several phytoconstituents especially the abundance of aromatic hydrocarbons on the nanosurface. Hence, the FTIR analysis confirms the biofunctionalization of the AgNPs.

Field emission scanning electron microscopy (FESEM) and energy-dispersive X-ray spectroscopy (EDX)

Scanning electron microscopy was used to examine the nanoparticle's size, shape, and distribution. Figure 6 shows the SEM images of synthesized AgNPs after alcohol washing. The images support several other reports that describe the synthesis of spherically shaped, mono-dispersed nanoparticles. The average size of the nanoparticles from the SEM analysis was determined to be in the range of 80–100 nm.

The elemental composition of the synthesized AgNPs was determined through EDX analysis. As depicted in Fig. 7, two strong intensity peaks have been observed due to scattering from K shell and L shell of silver atoms signifying the formation of AgNPs.

The peaks from C and O atoms signifying the presence of phytoconstituents on the nanosurface. The abundance of O atoms in the EDX analysis also signifies the partial oxidation of AgNPs into silver oxide (Ag_2O). The presence of Au is due to the sputter coating.

Dynamic light scattering (DLS)

Dynamic light scattering (DLS) also known as photon correlation spectroscopy (PCS) has been used for determining the sizes and shapes of nanoparticles in liquids. The time variations in the amount of light scattered by the particle dispersion are tracked and recorded. The ability to detect the light scattered as a result of light's interaction with matter provides details on the sample's physical properties. According to the dynamic light scattering study size distribution profile, the hydrodynamic diameter of these bio-synthesized silver nanoparticles was calculated. As depicted in Fig. 8, 96.8% intensity was associated with peak 1 having average hydrodynamic diameter of 212.1 nm. Another two small peaks, 2.7 and 0.5 percentage of intensity were associated with peak 2 and peak 3 having average hydrodynamic diameters of 27.26 and 8.584 nm, respectively. From this data, the average hydrodynamic diameter was determined to be 152.5 nm that is also in accordance with our SEM data. The hydrodynamic diameter of silver nanoparticles determined by DLS study was 152.5 nm. The average diameter determined by SEM image was near about 100 nm. This is because, during SEM study only one particular section is being focused. Hence, the standard error of measurement is high, whereas DLS deals with millions of particles simultaneously and also their surface chemistry. Hence, the

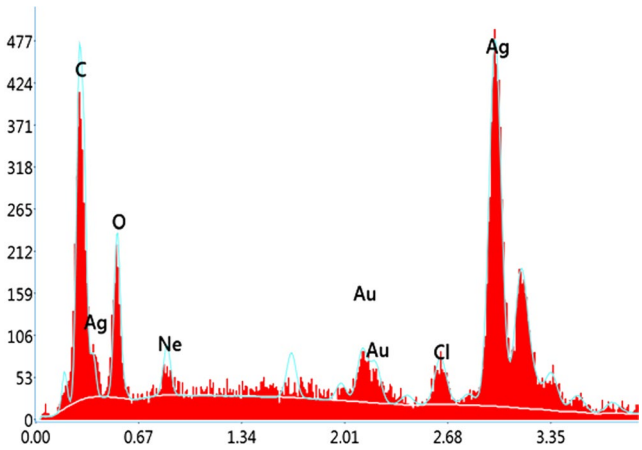

Fig. 7 Energy-dispersive X-ray analysis of biofunctionalized AgNPs

Element	Weight %	Atomic %	Error %	Net Int.
C K	10.82	36.86	11.72	28.89
O K	11.90	30.43	14.23	18.61
Ne K	1.64	3.32	21.79	6.40
Cl K	2.35	2.71	21.47	6.90
Ag L	66.88	25.35	7.13	80.65
Au M	6.41	1.33	14.56	9.65

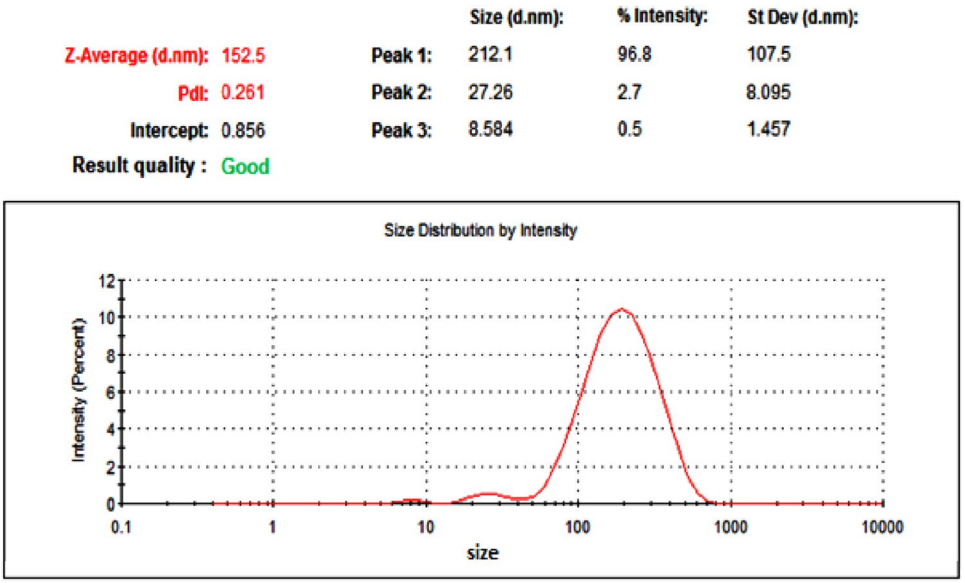

Fig. 8 Dynamic light scattering analysis of biofunctionalized AgNPs

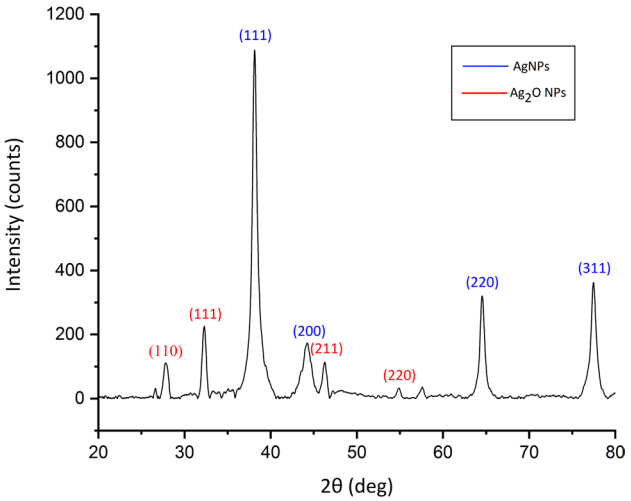

Fig. 9 X-ray diffraction pattern for biofunctionalized AgNPs

hydrodynamic diameter is expected to be greater than the average diameter depicted in SEM image. The hydrodynamic diameter also demonstrates the stability of the colloidal suspension. The smaller the hydrodynamic diameter, the greater stability of the nanoparticles that enhances the antibacterial efficacy and shelf life of the nanoparticles.

X-Ray diffraction analysis (XRD)

The XRD pattern of the synthesized biofunctionalized AgNPs has confirmed the crystalline nature of AgNPs.

The diffractogram as depicted in Fig. 9 has been compared to the standard powder diffraction card of JCPDS, silver file number 00-004-0783. Four Bragg refraction peaks were observed that can be indexed to (111), (200), (220) and (311) planes of face-centre cubic silver having 2θ values of 38.18, 44.28, 64.52 and 77.51 degrees, respectively, that confirms the presence of silver nanoparticles. Four other minute peaks have also been observed at 27.82, 32.34, 46.28, 54.89 can be corroborate with (110), (111), (211), (220) planes of silver oxide (JCPDS 76–1393). The XRD pattern of the synthesized AgNPs has shown diffraction peaks with similar 2θ values that is evident in recent studies (Fatemeh et al. 2017), confirming the presence of AgNPs crystals.

Evaluation of cytotoxicity on RAW 264.7macrophages

The cytotoxicity assay was carried out on RAW 264.7 macrophages using different concentrations of gentamicin, plant extract and biofunctionalized AgNPs as mentioned earlier in the materials and method section. When the cell lines (10^4 cells/well) were treated with AgNPs of 5, 2.5, 1.25 and 0.625 µg/ml concentrations, the percentages of survivability were observed to be 39.76, 43.49, 57.48 and 75.7, respectively (Fig. 10a). Whereas it has been observed upon treatment with 0.5, 0.25, 0.125 and 0.063 µg/ml of Gentamicin, 74.07, 77.43, 85.43 and 95.86 per cent of cells survived (Fig. 10b). When the macrophages were treated with 250, 125, 62.5 and 31.25 µg/ml of plant extract, the percentages of survivability were observed to be 50.54, 63.8, 74.04 and 79.22, respectively (Fig. 10c).

From the above-mentioned data, the IC50 value for AgNPs and Plant extract were determined to be approximately 1.875 and 250 µg/ml, respectively. This signifies the AgNPs is 133.33 times toxic compared to plant extract against RAW 264.7 macrophages (Table 1). It has been reported that the IC50 values of green synthesized AgNPs on

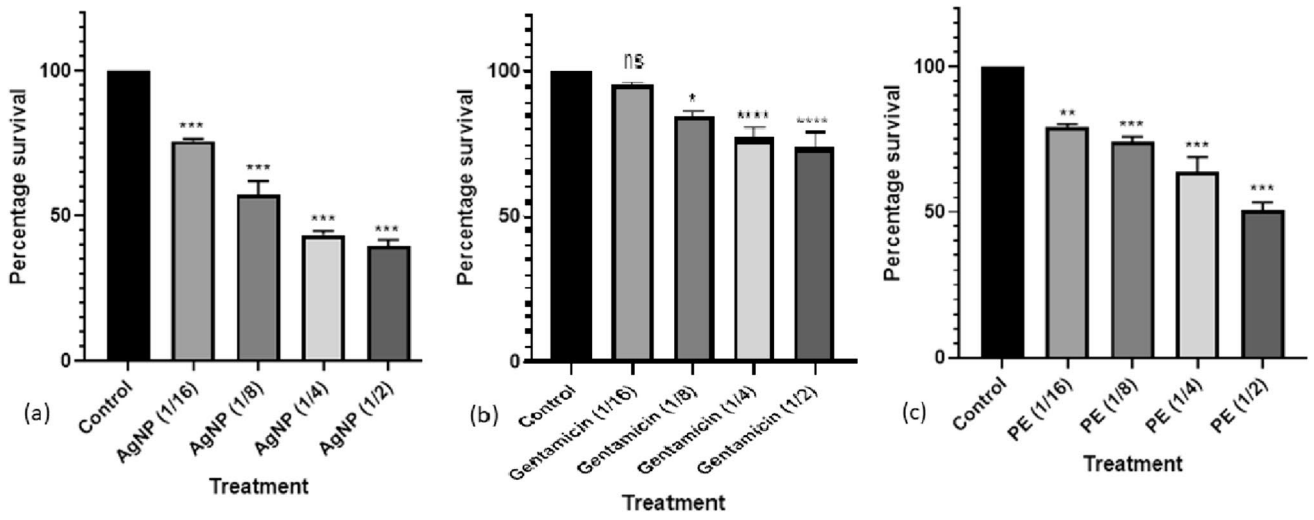

Fig. 10 Evaluation of cytotoxicity of AgNPs (**a**), Gentamicin (**b**) and Plant Extract (**c**) on RAW 264.7 macrophages by MTT assay. ^{ns}Not significant; *p value < 0.05; **p value < 0.01; ***p value < 0.001; ****p value < 0.0001

Table 1 Assessment of RAW 264.7 macrophages survivability by MTT Assay

Dilution Factor	Percentage of survivability			
	Control	AgNPs (10 µg/ml)	Gentamicin (1 µg/ml)	Plant extract (500 µg/ml)
1/2th	100	39.76	74.07	50.54
1/4th	100	43.49	77.43	63.80
1/8th	100	57.48	85.43	74.04
1/16th	100	75.70	95.86	79.22

G292, HCT-116, MCF-7, MDAMB-231 and Hep-G2 were 3.42, 1.4, 2.1, 6 and 1.2 µg/ml, respectively (Suleiman et al. 2015; Gurunathanet al. 2013). Our cytotoxicity analysis data are in tandem with the previously reported data and signifies the biofunctionalized AgNPs exerts minimal detrimental effect on human cell line though having good antibacterial efficacy. The high IC50 value of the plant extract against the above-mentioned cell line also signifies that biofabrication of the phytoconstituents increases the bio-compatibility of the AgNPs. However, the IC50 value of the biofunctionalized AgNPs should be higher to make it feasible and more bio-compatible for in vivo studies.

Gas chromatography–Mass spectrometry (GC–MS):

The molecules attached to the nanosurface have been recovered and subjected to GC–MS analysis. The identified molecules and their plausible roles are summarized in Table 2. The roles of the phytochemicals have been demonstrated in recently reports as antibacterial, antifungal and anti-inflammatory agents. This result suggests that the phytochemicals not only increases the biocompatibility of the nanoparticles but also enhances the antibacterial efficacy.

Table 2 Gas chromatography–Mass spectrometry analysis of the phytochemicals capping the AgNPs

Serial number	Name of the compounds	Molecular weight	Biological activities
1	Dotriacontane	450	Antibacterial (Kawuri and Darmayasa 2019)
2	Tetratetracontane	618	Antibacterial (Kawuri and Darmayasa 2019)
3	Tetracontane	562	Antibacterial (Kawuri and Darmayasa 2019)
4	Heneicosane	296	Antibacterial and antifungal (Vanitha et al. 2020)
5	Eicosane	282	Antibacterial (Naeim et al. 2020)
6	Benzenepropanoic acid, 3,5-bis(1,1-dimethylethyl)-4-hydroxy-, ethyl ester	306	Antifungal and antioxidant (Belakhdar et al. 2015)
7	4-(3,5-Di-tert-butyl-4-hydroxyphenyl)butyl acrylate	332	Antifungal and antioxidant (Belakhdar et al. 2015)
9	Triacontane, 1-iodo	548	Antibacterial (Kawuri and Darmayasa 2019))

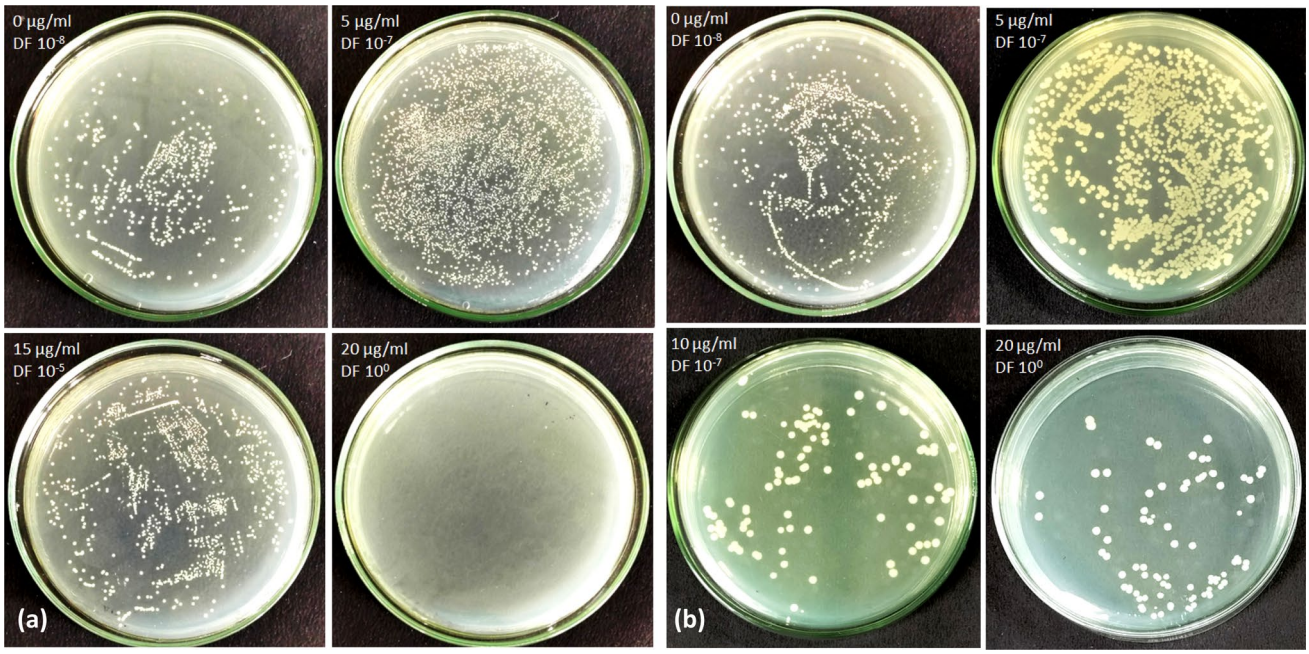

Fig. 11 Evaluation of antibacterial efficacy of biofunctionalized AgNPs against *Bacillus cereus* (**a**) and *Escherichia coli* (**b**)

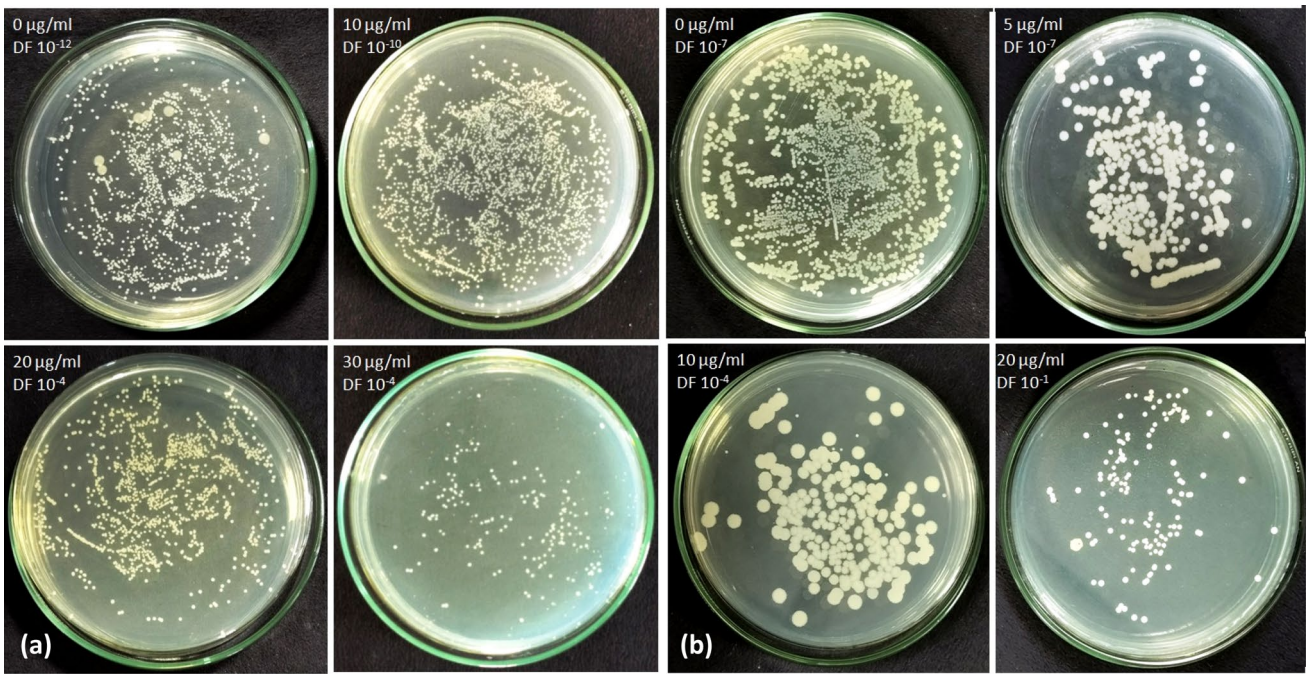

Fig. 12 Evaluation of antibacterial efficacy of biofunctionalized AgNPs against *Staphylococcus aureus* (**a**) and *Vibrio cholerae* (**b**)

Antibacterial activity of AgNPs

To evaluate the antibacterial efficacy of the AgNPs, broth dilution method was performed followed by spreading on agar plates as depicted in Figs. 11 and 12. The minimum bactericidal concentration (MBC) was calculated by determination of the lowest concentration of AgNPs which reduces the bacterial population to 99.9% (Table 3).

In this study, it has been determined the MBC values of AgNPs were 20, 20, 10 and 20 µg/ml against *Bacillus cereus*, *Staphylococcus aureus*, *Vibrio cholerae*, and *Escherichia coli.* The same against gentamicin were determined to be

Table 3 Survivability of four strains after treatment with biofunctionalized AgNPs, plant extract and gentamicin

Strains	Concentration of AgNPs (µg/ml)	(CFUs/0.05 ml) × dilution factor	Percentage of survivability	Concentration of plant extract (µg/ml)	(CFUs/0.05 ml) × dilution factor	Percentage of survivability	Concentration of gentamicin (µg/ml)	(CFUs/0.05 ml) × dilution factor	Percentage of survivability
Bacillus cereus	0	507×10	100	0	507×10^{8}	100	0	507×10^{8}	100
	5	2321×10^{7}	45.78	625	20×10^{9}	39.44	1.25	1232×10^{5}	0.24
	15	1440×10^{5}	0.28	1875	13×10^{9}	25.64	**2.5**	29×10^{4}	0.001
	20	0	0	2500	16×10^{9}	31.56	3.75	21×10^{2}	0
Staphylococcus aureus	0	1564×10^{12}	100	0	1564×10^{12}	100	0	1564×10^{12}	100
	10	3544×10^{10}	2.27	625	1488×10^{12}	95.14	**1.25**	8×10^{8}	0
	20	1046×10^{4}	0	1250	1394×10^{12}	89.13	2.5	1846×10^{5}	0
	30	182×10^{4}	0	2500	945×10^{12}	60.4	3.75	31×10^{5}	0
Vibrio cholerae	0	2183×10^{7}	100	0	2183×10^{7}	100	0	2183×10^{7}	100
	5	363×10^{7}	16.63	625	8×10^{9}	36.6	**1.25**	82	0
	10	267×10^{4}	0.01	1250	25×10^{8}	11.4	2.5	5	0
	20	153×10	0	1875	17×10^{8}	7.79	3.75	0	0
Escherichia coli	0	1084×10^{8}	100	0	1084×10^{8}	100	0	1084×10^{8}	100
	5	1343×10^{7}	12.39	625	48×10^{9}	44.3	1.25	1517×10^{6}	1.4
	10	112×10^{7}	1.03	1250	33×10^{9}	30.44	**2.5**	1615×10^{4}	0.01
	20	82	0	**1875**	1×10^{10}	9.22	3.75	1×10^{4}	0

*The MBC values are depicted in bold letters

2.5, 1.25, 1.25 and 2.5 µg/ml for the four strains mentioned above, respectively. The plant extract has also shown antibacterial activity against all the four strains at significantly higher doses compared to AgNPs. For instance, 20 µg/ml of AgNPs reduces the entire *Bacillus cereus* cell population but even within the same cell population with 2500 µg/ml plant extract treatment reduces the population by 68.44%.

However, the antibacterial activity of plant extract was significantly higher against *E. coli* in comparison to other strains. This signifies that when the AgNPs is coated with phytoconstituents, the antibacterial efficacy was further enhanced. This validates the role of phytoextract not only in the synthesis of nanoparticle but also in elevation of the antibacterial efficacy as reflected in the survivability plot (Fig. 13) where the slop of AgNPs is significantly greater than that of the plant extract (Supplementary Fig. 3). As depicted in Supplementary Figs. 1, 2, the antibacterial efficacy of AgNPs was found to be 6.25% of that of gentamicin against *Staphylococcus aureus* and 12.5% for rest of the strains. This study reveals that biofunctionalized AgNPs has significant antibacterial efficacy and bio-compatibility. It has reported AgNPs demonstrate their potential as antibacterial agents through a variety of ways. The most notable forms of antimicrobial action of AgNPs have been identified as adherence to microbial cells, penetration inside the cells, formation of ROS and free radicals, and regulation of microbial signal transduction pathways. Parvekar et al. (2020) has reported that the MBC value of AgNPs against *S. aureus* was 0.625 mg/ml. Bakht Dalir et al. (2020) has reported that AgNPs has MBC values in the range of 0.875–3.5 mg/ml against four bacterial strains. Hence, our biofunctionalized AgNPs have shown to be more effective as compared to the recent studies. This may be attributed to the surface functionalization of the AgNPs.

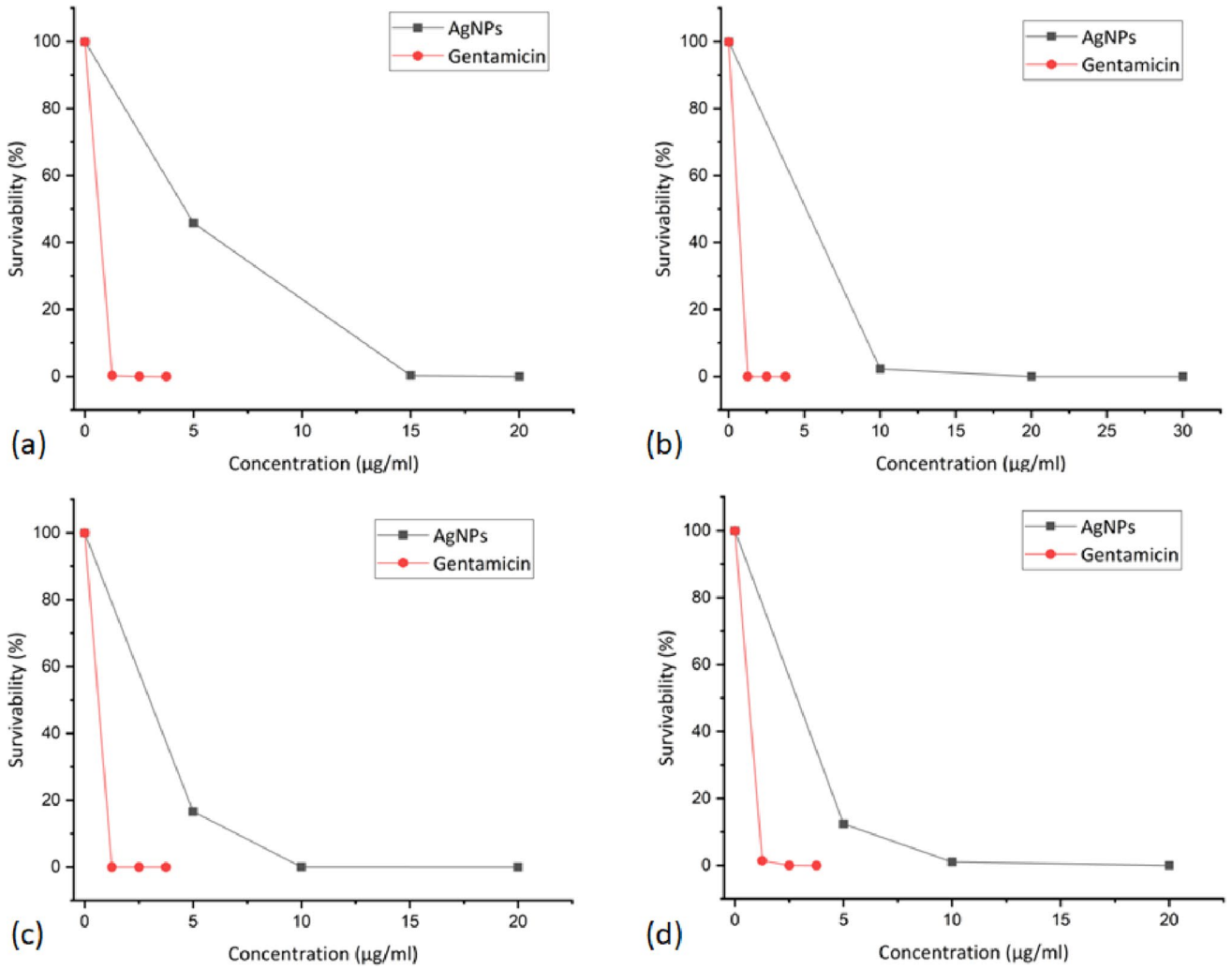

Fig. 13 Survivability plot of *Bacillus cereus* (**a**) *Staphylococcus aureus* (**b**) *Vibrio cholera* (**c**) *Escherichia coli* (**d**) followed by treatment with biofunctionalized AgNPs and gentamicin

Experimental

Materials

Clerodendrum glandulosum leaves were collected in the monsoon season from West Bengal, India. The bacterial pure cultures of *Bacillus cereus* (MTCC 9817), *Staphylococcus aureus* (MTCC 7443), *Vibrio cholerae* (MTCC 3906) and *Escherichia coli* (MTCC 443) were collected from University of Calcutta, India. Silver nitrate (Merck, India), Luria broth (HiMedia, India) and ethyl alcohol (SRL, India) have been used in this study. All the materials purchased were of the highest standards of purity and quality for analysis. Aqua regia (3:1 HCl/HNO_3, SRL, India) was used to carefully clean the glassware (Borosil, India).

Extraction of plant material

The *Clerodendrum glandulosum* leaves were thoroughly washed with distilled water followed by drying and grinding into powder. In a 250 ml glass beaker, 5 g of leaf powder was added to 100 ml of distilled water in a 250 ml glass beaker and heated at 65 °C for 30 min on a hotplate until it turns pale brown in colour. The solution was allowed to cool at room temperature followed by filtration

through Whatman filter paper grade no. 1 to remove any coarse material. The pH of the purified leaf extract was recorded to be 5.51. In order to be used for future experiments, the extract was stored at a 4 °C temperature.

Synthesis of biofunctionalized AgNPs

The bottom-up approach was used to carry out the synthesis of silver nanoparticles (AgNPs) by simple aqueous reduction and precipitation method with modification with the method reported earlier (Agrawal et al. 2022). To start with, 135.2 mg of Silver nitrate ($AgNO_3$) was dissolved into 5 ml of distilled water in a 250 ml flask and was placed on a hotplate into which 25 ml of plant extract was gradually added under continuous shaking at 500 rpm at 65 °C temperature. The initial pH of the reaction mixture was recorded to be 5.08. The reaction was allowed to continue for 90 min. The reaction mixture was started to darken from 15 min and eventually turned into colloidal dark brown, indicating the reduction of Ag^+into elemental silver (Ag^0). The final pH of the reaction mixture was recorded to 4.52. In order to allow the silver nanoparticles to settle, the reaction mixture was left at room temperature for overnight. On the following day, the top layer of the obtained suspension was carefully discarded. The suspension was then centrifuged at 12,000 rpm for 15 min. The supernatant was carefully discarded and the pellet was dissolved in distilled water. The brownish black suspension was thoroughly rinsed three times with double-distilled water to get rid of any leftover contaminants. After being sonicated to create mono-dispersed nanoparticles, any unreacted remaining organic material was washed away once with 50, 70, or 90% alcohol subsequently. The pellet was then allowed to dry for 2–3 h in a hot air oven at 80 °C temperature. Before characterization and applications, the dried silver nanoparticles were kept in desiccators to get rid of any trace of leftover solvent. Reactions were initially conducted under various sets of conditions in order to optimize the reaction conditions.

UV–visible spectrophotometry

UV–visible spectrophotometry (UV-1800 Shimadzu spectrophotometer) was used in order to confirm the formation of AgNPs and to further investigate the mono-dispersity and size variability (Kumar et al. 2017). The UV–visible spectra were recorded in the range of 375–700 nm taking water as blank. To optimize the reaction conditions, the synthesis of the nanoparticles was conducted at various pH, incubation temperatures and concentration ratios (plant extract to silver nitrate solution). UV–visible spectrophotometry was used to further investigate the end product of each reaction set at different time intervals to confirm the optimization.

Fourier transform infrared spectroscopy (FTIR)

The chemical composition of the synthesized biofunctionalized AgNPs was investigated using Fourier transform infrared (FTIR) spectrometry in the 400–4000 cm^{-1} range. The samples were prepared using the potassium bromide (KBr) pellet technique (Antonow et al. 2004). Pellets were created by mixing KBr with AgNPs powder and plant extract under hydraulic pressure. Each sample's background noise was recorded from pure KBr pellet. The data processing and baseline corrections have been done using the Origin 8.5 software.

Field emission scanning electron microscopy (FESEM)

In order to study the shape and size variability, scanning electron microscopy (Schottky, JSM-7610F) was performed. During the sample preparation, the AgNPs sample was sputter-coated with an ultra-thin layer (20 nm) of electrically conducting gold/palladium (Au/Pd) metals due to its semiconductivity. Sputter coating prevents the charging of the sample brought about by the buildup of static electric fields. By increasing the quantity of secondary electrons emitted from the specimen's surface, sputter coating also raises the signal-to-noise ratio, increasing the resolution of the image. The specimen was subjected to 10 keV electron beam bombardment at 35,000 × magnification (Arshadi-Rastabi et al. 2015). Energy-dispersive X-ray spectroscopy (EDX) that is equipped with SEM was used to study the elemental composition of the synthesized biofunctionalized nanoparticles.

Dynamic light scattering (DLS)

By detecting the dynamic fluctuations in light scattering intensity brought on by the Brownian motion of the particles, dynamic light scattering was used to determine the size distribution of the particles. The measurement provided the hydrodynamic diameter distribution peak values, the polydispersity index (PdI), which indicated the width of the particle size distribution and the average hydrodynamic diameter of the particles. A temperature equilibrium time of 1 min at 25 °C was used for all measurements, which were performed in triplicates. The diluted sample of the synthesized nanoparticle suspension (1 mg/ml) was allowed to filter through a 0.22-µm syringe-driven filter before DLS study.

X-ray diffraction analysis (XRD)

The presence of AgNPs, crystalline nature, phase variety and grain size were determined using X-ray diffraction analysis. The XRD analysis (Pan Analytical, X-pert pro, Netherland)

of the purified AgNPs powder was carried out using Cu-Kα radiation source in scattering range m(2θ) of 20–80 degrees on the instrument operating at a voltage of 45 kV and current flow at 40 mA.

Cytotoxicity in RAW 264.7 macrophages

Murine Macrophage like tumour cell, RAW 264.7 was cultured and maintained in complete DMEM medium supplemented with 10% FBS at 37˚C in 5% CO_2 atmosphere. For cytotoxic evaluation, Raw 264.7 macrophages (10^4cells/well) were plated in 96-well cell culture plates and incubated with different concentrations of AgNPs, gentamicin and plant extract for 48 h. After incubation, 20 µl 3-(4,5-dimethylthiazol-2-yl)-2,5-diphenyl tetrazolium bromide (MTT) reagent (5 mg/ml) was added to each well and incubated in dark for 3 h in CO_2 incubator. Then the culture media were removed and MTT formazan crystals were dissolved using 100 µl of DMSO. The absorbances were recorded at 595 nm. Thus, cell viability was determined by the MTT assay and the 50% cytotoxic concentrations (IC50) were calculated for AgNPs, gentamicin and plant extract.

Gas chromatography–mass spectrometry (GC–MS)

Identification of bioactive molecules adsorbed to the surface of nanoparticles was carried out using GC–MS (GCMS-QP2020 NX, Shimadzu) with SH-Rtx-5 diphenyl dimethyl polysiloxane (5%) stationary phase column (thick-ness: 0.25 µm, length: 30.0 µm, diameter: 0.25 mm) equipped with FID detector. The sample of biofunctionalized AgNPs was kept overnight in absolute ethanol at room temperature for detachment of the phytochemicals from the nanosurface followed by centrifugation at 12,000 rpm for 15 min. The phytochemicals were retained in the supernatant and transferred into a fresh vial. The phytochemical sample was then run through GC–MS at a range of 50–650 *m/z*. Helium was used as the carrier gas at flow rate of 1 ml/min and the injection volume was 1 µl. The oven temperature was initially maintained at 40 °C for 3 min and then raised to 280 °C at the rate of 5 °C/min. The injector and detector temperatures were set at 220 and 290 °C, respectively.

Antibacterial efficacy of AgNPs

The antibacterial assay for the evaluation of antibacterial activity of biofunctionalized AgNPs has been done by broth dilution method following (Dhara et al. 2022) with slight modification against two gram positive bacteria (*Bacillus cereus* and *Staphylococcus aureus*) and two gram negative bacteria (*Escherichia coli* and *Vibrio cholerae*) in different sets of culture tubes (one set each for AgNPs, gentamicin and plant extract treatment for each of the individual strain). In each tube, 4 ml of Luria broth and 8 µl of fresh bacterial culture was added followed by treatment with AgNPs, gentamicin and plants extract at different doses as depicted in table depicted in Table 1. One bacterial culture from each set has not been treated with AgNPs, gentamicin or plant extract, was taken as control. After treatment, the culture tubes were incubated under optimum conditions in shaking incubator for 12 h. After incubation, the cultures were diluted accordingly (Table 1) in order to obtain countable CFUs and spread on LB agar plates followed by incubation under optimum conditions. On the following day, the CFUs are counted and the percentage of survivability was calculated for each treatment by taking the ratio of CFUs of experimental set to that of the control set. The MBC values of AgNPs and gentamicin were calculated from the survivability percentage that is the concentration of the antibacterial agents against which the survivability of bacteria is less than or equal to 0.1%.

Conclusion

In this study, we focused to synthesize silver nanoparticles using an environmental-friendly and cost-effective strategy as first step to solve global challenge of antibiotic resistance. *Clerodendrum glandulosum* has been well recognized for its medicinal values but not scientifically validated. The proposed route of synthesis of silver nanoparticles and simultaneous capping of bioactive phytoconstituents provides an efficient and sustainable method to obtain well dispersed spherical AgNPs of average diameter of 80–100 nm. The synthesized nanoparticles gave absorption maxima at 450 nm due to its characteristic surface plasmon resonance. The presence of bioactive phytoconstituents on the nanosurface as evident from EDX and FTIR spectroscopic analysis enhances the antibacterial efficacy and biocompatibility of the nanoparticles. The synthesized biofunctionalized AgNPs shown to have high bactericidal activity which could be attributed to their ability of ROS and free radical generation, modulation of various signal transduction pathways. The MBC values of the AgNPs against gram positive (*Bacillus cereus* and *Staphylococcus aureus*) and gram negative (*Escherichia coli* and *Vibrio Cholerae*) were determined to be 20, 20, 20 and 10 µg/ml, respectively, which is highly in significance with the recent studies revealing the effectiveness of our biofunctionalized AgNPs. The synthesized AgNPs from *Clerodendrum glandulosum*has shown to have stability and significant antibacterial efficacy with minimum detrimental effect on healthy human cells (IC50 value of 1.875 µg/ml against RAW 264.7 macrophages). This study and similar strategies could unveil new paths in antibacterial chemotherapy.

Acknowledgements We would like to express our sincere thanks to University of Calcutta for providing bacterial inoculum. We would also like to express our gratitude to Central Instrumental Facility, IOC-ICT, Bhubaneshwar, for providing the SEM and GC-MS facility. We would like to express our sincere thanks to Professor Parimal Karmakar and Ashik Iqbal of Jadavpur University for helping in nanoparticle characterization part. Dr. Mohd Afzal extends his appreciation to researchers supporting project number (RSPD2024R979), King Saud University, Riyadh, Saudi Arabia, for financial assistance.

Author's contributions Manmata Dhara has conceptualized and executed the study, written and reviewed the manuscript. Rubina Khatun, Supriya Mandal and Aditi Mondal have done the experimental works and written the manuscript. Dr. Junaid Jibran Jawed, Dr. Nazia Kausar, Dr. Abdulla Al Masum, Mohd Afzal and Maria Christy have conceptualized and supervised the work, reviewed and finalized the manuscript. All authors were involved in the critical review and finalizing the paper.

Declarations

Conflict of interest The authors declare that they have no known competing financial interests or non-financial interests that could have appeared to influence the work reported in this paper.

References

Adil M, Bashir S, Bashir S, Aslam Z, Ahmad N, Younas T, Asghar RM, Alkahtani J, Dwiningsih Y, Elshikh MS (2022) Zinc oxide nanoparticles improved chlorophyll contents, physical parameters, and wheat yield under salt stress. Front Plant Sci 13. https://doi.org/10.3389/fpls.2022.932861

Agrawal G, Sarkar B, Saha R (2022) 187 Green synthesis of silver nanoparticles from leaves of *Clerodendrum glandulosum* Lindl. and evaluation of its antimicrobial and antioxidant activities. Int J Pharm Chem8 (Supplement).

Ahmad N, Sharma S, Singh VN, Shamsi SF, Fatma A, Mehta BR (2011) Biosynthesis of silver nanoparticles from *Desmodium triflorum*: a novel approach towards weed utilization. Biotechnol Res Int. https://doi.org/10.4061/2011/454090

Alavi M, Rai M (2019) Recent advances in antibacterial applications of metal nanoparticles (MNPs) and metal nanocomposites (MNCs) against multidrug-resistant (MDR) bacteria. Expert Rev Anti Infect Ther 17(6):419–428. https://doi.org/10.1080/14787210.2019.1614914

Antonow D, Graebin CS, Eifler-Lima VL (2004) An efficient monitoring technique for solid-phase reactions by KBr pellets/FT-IR using methyl p-aminobenzoate synthesis assisted by microwave radiation on merrifield resin. J Braz Chem Soc 15:782–785. https://doi.org/10.1590/S0103-50532004000500028

Arshadi-Rastabi S, Moghaddam J, Eskandarian MR (2015) Synthesis, characterization and stability of Cu_2O nanoparticles produced via supersaturation method considering operational parameters effect. J Ind Eng Chem 22:34–40. https://doi.org/10.1016/j.jiec.2014.06.022

Aziz A, Khalid M, Akhtar MS, Nadeem M, Gilani ZA, Asghar HU, Rehman J, Ullah Z, Saleem M (2018) Structural, morphological and optical investigations of silver nanoparticles synthesized by sol-gel auto-combustion method. Dig J Nanomater Biostructures 13(3).

Bakht Dalir SJ, Djahaniani H, Nabati F, Hekmati M (2020) Characterization and the evaluation of antimicrobial activities of silver nanoparticles biosynthesized from *Carya illinoinensis* leaf extract. Heliyon 6(3).

Belakhdar G, Benjouad A, Abdennebi EH (2015) Determination of some bioactive chemical constituents from *Thesium humile* Vahl. J Mater Environ Sci 6(10):2778–2783

Bharadwaj A, Rastogi A, Pandey S, Gupta S, Sohal JS (2022) Multidrug-Resistant Bacteria: their mechanism of action and prophylaxis. BioMed Res Int 5:2022

Bruna T, Maldonado-Bravo F, Jara P, Caro N (2021) Silver nanoparticles and their antibacterial applications. Int J Mol Sci 22(13):7202.

Dawadi S, Katuwal S, Gupta A, Lamichhane U, Thapa R, Jaisi S, Lamichhane G, Bhattarai DP, Parajuli N (2021) Current research on silver nanoparticles: synthesis, characterization, and applications. J Nanomater 5(2021):1–23

Dhara M, Kisku K, Naik UC (2022) Biofunctionalized cuprous oxide nanoparticles synthesized using root extract of *Withaniasomnifera* for antibacterial activity. ApplNanosci 17:1–7.https://doi.org/10.1007/s13204-022-02452-3

Fatemeh KO, Mohammad Javad MO, Samaneh KH (2017) The effect of silver nanoparticles on composite shear bond strength to dentin with different adhesion protocols. J Appl Oral Sci 25:367–373

Feng Y, Lin S, Huang S, Shrestha S, Conibeer G (2015) Can Tauc plot extrapolation be used for direct-band-gap semiconductor nanocrystals? J Appl Phys 117(12):125701. https://doi.org/10.1063/1.4916090

Gao Y, Chen Y, Cao Y, Mo A, Peng Q (2021) Potentials of nanotechnology in treatment of methicillin-resistant Staphylococcus aureus. Eur J Med Chem 213:113056. https://doi.org/10.1016/j.ejmech.2020.113056

Gouyau J, Duval RE, Boudier A, Lamouroux E (2021) Investigation of nanoparticle metallic core antibacterial activity: Gold and silver nanoparticles against *Escherichia coli* and *Staphylococcus aureus*. Int J of Mol Sci 22(4):1905.

Gurunathan S, Han JW, Eppakayala V, Jeyaraj M, Kim JH (2013) Cytotoxicity of biologically synthesized silver nanoparticles in MDA-MB-231 human breast cancer cells. Biomed Res. https://doi.org/10.1155/2013/535796

Hussain Z, Abourehab MA, Khan S, Thu HE (2020) Silver nanoparticles: A promising nanoplatform for targeted delivery of therapeutics and optimized therapeutic efficacy. In: Metal nanoparticles for drug delivery and diagnostic applications. Elsevier, Amsterdam, pp 141–173. https://doi.org/10.1016/B978-0-12-816960-5.00009-4

Ibrahim HM (2015) Green synthesis and characterization of silver nanoparticles using banana peel extract and their antimicrobial activity against representative microorganisms. J Radiat Res Appl Sci 8(3):265–275. https://doi.org/10.1016/j.jrras.2015.01.007

Kawuri R, Darmayasa IB (2019) Bioactive compound of *Streptomyces capoamus* as biocontrol of Bacterial Wilt Disease on Banana Plant. IOP Conf Ser Earth Environ Sci 347(1):012054.

Kumar B, Smita K, Cumbal L, Debut A, Angulo Y (2017) Biofabrication of copper oxide nanoparticles using Andean blackberry (*Rubus glaucus Benth*.) fruit and leaf. J Saudi Chem Soc 21:S475–S480. https://doi.org/10.1016/j.jscs.2015.01.009

Marimuthu S, Rahuman AA, Rajakumar G, Santhoshkumar T, Kirthi AV, Jayaseelan C, Bagavan A, Zahir AA, Elango G, Kamaraj C (2011) Evaluation of green synthesized silver nanoparticles against parasites. Parasitol Res 108:1541–1549. https://doi.org/10.1007/s00436-010-2212-4

Michael CA, Dominey-Howes D, Labbate M (2014) The antimicrobial resistance crisis: causes, consequences, and management. Front Public Health 2:145. https://doi.org/10.3389/fpubh.2014.00145

Mistry H, Thakor R, Patil C, Trivedi J, Bariya H (2021) Biogenically proficient synthesis and characterization of silver

nanoparticles employing marine procured fungi *Aspergillus brunneoviolaceus* along with their antibacterial and antioxidative potency. Biotechnol Lett 43:307–316. https://doi.org/10.1007/s10529-020-03008-7

Naeim H, El-Hawiet A, Abdel Rahman RA et al (2020) Antibacterial activity of Centaurea pumilio L. . root and aerial part extracts against some multidrug resistant bacteria. BMC Complement Med Ther 20:79. https://doi.org/10.1186/s12906-020-2876-y

Nguyen NP, Dang NT, Doan L, Nguyen TT (2023) Synthesis of silver nanoparticles: from conventional to 'modern' methods—a review. Processes 11(9):2617.

Parvekar P, Palaskar J, Metgud S, Maria R, Dutta S (2020) The minimum inhibitory concentration (MIC) and minimum bactericidal concentration (MBC) of silver nanoparticles against Staphylococcus aureus. Biomater Investig Dent 7(1):105–109.

Priya MM, Selvi BK, Paul JA (2011) Green synthesis of silver nanoparticles from the leaf extracts of *Euphorbia hirta* and *Nerium indicum*. Dig J Nanomater Biostructures (DJNB) 6(2).

Sharma HK, Chhangte L, Dolui AK (2001) Traditional medicinal plants in Mizoram. India Fitoterapia 72(2):146–161. https://doi.org/10.1016/S0367-326X(00)00278-1

Sharma VK, Yngard RA, Lin Y (2009) Silver nanoparticles: green synthesis and their antimicrobial activities. Adv Colloid Interface Sci 145(1–2):83–96. https://doi.org/10.1016/j.cis.2008.09.002

Singh J, Bhuyan TC, Ahmed A (1996) Ethnobotanical studies on the Mishing tribes of Assam with special reference to food and medicinal plant. Econ Bot 12:350–356

Suleiman M, Al-Masri M, Al Ali A, Aref D, Hussein A, Saadeddin I, Warad I (2015) Synthesis of nano-sized sulfur nanoparticles and their antibacterial activities. J Mater Environ Sci 6(2):513

Vanitha V, Vijayakumar S, Nilavukkarasi M, Punitha VN, Vidhya E, Praseetha PK (2020) Heneicosane—A novel microbicidalbioactive alkane identified from Plumbago zeylanica L. Ind Crop Prod 154:112748

World Health Organization. Global antimicrobial resistance surveillance system (GLASS) report: early implementation 2020.